scientific reports

Check for updates

OPEN

Removal of fluoride from groundwater using a zeolite A supported magnetite biochar composite

Tessema Derbe[1], Yitayew Tesfaye[2,3], Taju Sani[2,3]✉ & Enyew Amare Zereffa[4]

Prolonged consumption of excess fluoride concentration (> 1.5 mg/L) from groundwater notably poses serious health effects, including dental and skeletal fluorosis in the Rift Valley area of Ethiopia. In this study, a zeolite A supported magnetite biochar composite (Z-A/M-BC) was synthesized through a pyrolysis method for the removal of fluoride from groundwater. The as-synthesized adsorbent was characterized using FT-IR, PXRD, SEM–EDX, PZC, and BET analysis to identify the functional group, phase structure, surface morphology, elemental composition, surface charge distribution, and surface area, respectively. The pH_{ZPC} determination for Z-A/M-BC is found to be 6.75, suggesting a large portion of the adsorbent with pH less than this value becomes protonated and positively charged and thus is favorable for fluoride removal through electrostatic attraction. Interestingly, the BET analysis results also exhibited that the synthesized Z-A/M-BC composite had a high surface area of 496.17 m^2/g, which is accessible for capturing fluoride from groundwater. The adsorption study was commenced via optimization of reaction parameters: pH, adsorbent dose, initial concentration (C_o), and contact time. The highest fluoride removal efficiency (95.80%) and capacity (6.39 mg/g) were recorded at pH 5, 1.2 g/L of adsorbent dose, 6 h of contact time, and 10 mg/L of C_o. The removal performance of the Z-A/M-BC composite was also tested in a real sample of groundwater having 12.25 mg/L of fluoride C_o which was collected from Kenteri town, Ethiopia. It was found to be 88.98% removal efficiency and 7.27 mg/g capacity, respectively. At last, the reusability study was conducted for 5 successive runs and found 95.80%, 90.40%, 87.30%, 85.40%, and 70.20% removal efficiency for the first, second, third, fourth, and fifth cycles, respectively. These confirm that the Z-A/M-BC adsorbent is promising for the removal of fluoride from groundwater at a large scale.

Keywords Adsorbent, Composite, Groundwater, Fluoride, Removal

Fluorine is well known for its high electron affinity and reactivity and is frequently found as fluoride ions. Fluoride is present in various minerals such as fluorite, fluorapatite, biotite, cryolite, and topaz[1]. Wastes discharged into surface and groundwater from various industries, such as fertilizer, electroplating, semiconductor, glass, and ceramics industries, also increase the amount of fluorides in surface and groundwater above the permissible level set by the World Health Organization (WHO)[2]. According to the WHO guidelines, the maximum acceptable limit of fluoride in drinking water is 0.5 to 1.5 mg/L[3]. Within the limit, fluoride is vital for the prevention of tooth decay and supports the proper growth of bone structure in human beings[1,4]. However, beyond the threshold limit, fluoride leads to various diseases, including skeletal and teeth fluorosis[3], joint stiffness[5], paralysis, thyroid dysfunction, and other gum diseases[1,3,6]. The problem spreads throughout the globe, specifically in many tropical and subtropical countries, including Libya, Iran, China, Iraq, South Africa, Kenya, and Ethiopia. In Ethiopia[6], particularly in the Rift Valley areas, the problem is getting worse. For instance, the research work conducted by Ebsa[7] shows the high fluoride concentration ranging from 3.8 mg/L to 12.7 mg/L in the Ziway district. According to Fito et al. report[8], the concentration of fluoride in the Rift Valley of Ethiopia also ranges from 5 to 26 mg/L, which is significantly higher than the limits set by WHO. Similarly, contemporary research

[1]Department of Chemistry, Wachemo University, P.O. Box 667, Hossana, Ethiopia. [2]Department of Industrial Chemistry, Addis Ababa Science and Technology University, P.O. Box 16417, Addis Ababa, Ethiopia. [3]Nanotechnology Center of Excellence, Addis Ababa Science and Technology University, P.O. Box 1647, Addis Ababa, Ethiopia. [4]Department of Applied Chemistry, School of Applied Natural Science, Adama Science and Technology University, P.O. Box 1888, Adama, Ethiopia. ✉email: taju.sani@aastu.edu.et

conducted by Gómez-Hortigüela and his co-workers also confirms the presence of high fluoride concentrations (> 5 mg/L) in the Rift Valley and lowland areas of Ethiopia[1]. Accordingly, reducing the fluoride concentration in potable water below WHO guidelines is being demanded and due substantial attention.

To date, numerous removal methods, including chemical precipitation[9], membrane separation[10,11], ion exchange[12], and adsorption[13], are widely used for the removal of fluoride. Most of them suffered with high costs, complicated procedures, usage of toxic chemicals, and low recovery[9,13]. For instance, the chemical precipitation consumes large chemicals and generates secondary pollutant (sludge) which has adverse effects on human health and aquatic life[11,14]. An ion-exchange is vulnerable to the interference of other ions[15,16]. Besides, it is relatively costly, and mostly limited on isoelectronic ions[13]. Membrane-based methods such as reverse osmosis, electrodialysis, and nanofiltration are highly effective for the removal of contaminates, however the method is complicated, costly, and suffers from membrane fouling, which is impractical for developing countries and rural areas[11,17]. Consequently, adsorption is found to be desirable for developing countries owing to its cost-effectiveness, simplicity to operate, and environmental friendliness[1,10,14]. Moreover, it uses a wide range of adsorbent materials such as zeolite, activated carbon, biochar, polymer, hydroxyapatite, and metal–organic frameworks (MOFs) for the defluoridation of groundwater[3,14,15]. Herein, the Z-A/M-BC composite and its pristine adsorbents were tested for the removal of fluoride from groundwater.

Zeolites are crystalline aluminosilicates, which consist of aluminum and silicon atoms bonded through bridging oxygen atoms to adopt a tetrahedral framework (TO_4, T = Si, or Al)[16]. The structure and porosity (Fig. 1a) of zeolites provide a good occasion for further modification with suitable motifs to develop efficient adsorbents for various applications[1]. Zeolite-A (Z-A) is the most common zeolite family, having high Al content and high cationic exchanger ability[17]. Due to its extensive sources, stability, large surface area, and obtainability, Z-A is used for the adsorption of cationic pollutants like heavy metals[17]. However, Z-A has a net negative charge at the Al metal center (Fig. 1b), which rendered the application of Z-A for the removal of fluoride from contaminated water[1,17,18] due to columbic repulsive force.

Biochar (BC) is one of the most popular environmentally friendly and low-cost porous materials for the adsorption of pollutants[21,22]. BC has received much attention owing to its high carbon content, surface-enriched chemistry, and stable structure[11,18,19]. Nevertheless, it possesses disordered structures, non-uniform sizes, and lacks recyclability, which creates secondary pollutants after adsorption[12,21]. These downsides will greatly limit the applications of BC for the removal of fluoride, which needs magnetization with magnetic materials. Magnetite (Fe_3O_4) is an inverted spinel possessing high chemical stability, high coercivity, excellent chelation behavior, and high selectivity towards fluoride adsorption[19,22]. Thus, designing adsorbent materials with high adsorption efficiency and recyclability is highly demanded.

In the present study, a Z-A/M-BC composite was synthesized for the removal of fluoride from groundwater. In the Z-A/M-BC composite, Z-A provides structural stability of the synthesized adsorbent[17]; Fe_3O_4 enhances the recovery and the defluoridation efficiency of the Z-A/M-BC composite. BC also conveys the functionality and active sites for fluoride removal in Z-A/M-BC composite. Thus, compositing Z-A and M-BC enhances the defluoridation efficiency of Z-A/M-BC composite. The defluoridation studies were commenced by optimization of sorption factors such as pH, adsorbent dose, C_o, and adsorption time. Besides, the Box-Behnken model was also applied using Design Expert 13 software to study the mutual interaction effects of contact time, C_o, and adsorbent dose during defluoridation of groundwater.

Materials and method

Chemicals and reagents

Analytical graded chemicals: $FeCl_2.4H_2O$, 99% and $FeCl_3.6H_2O$, 97% was supplied by Sisco Research Laboratories Pvt. Ltd., Delhi, India. C_2H_6O (96%, *Sigma-Aldrich*), NaOH (98%, *Merck*), DMF (99%, *Merck*), $CH_3COOC_2H_5$ (99%, *Merck*), HCl (37%, *Sigma- Aldrich*), NaCl (99.5%, *Maharashtra, India*), $Na_3C_6H_5O_7.2H_2O$

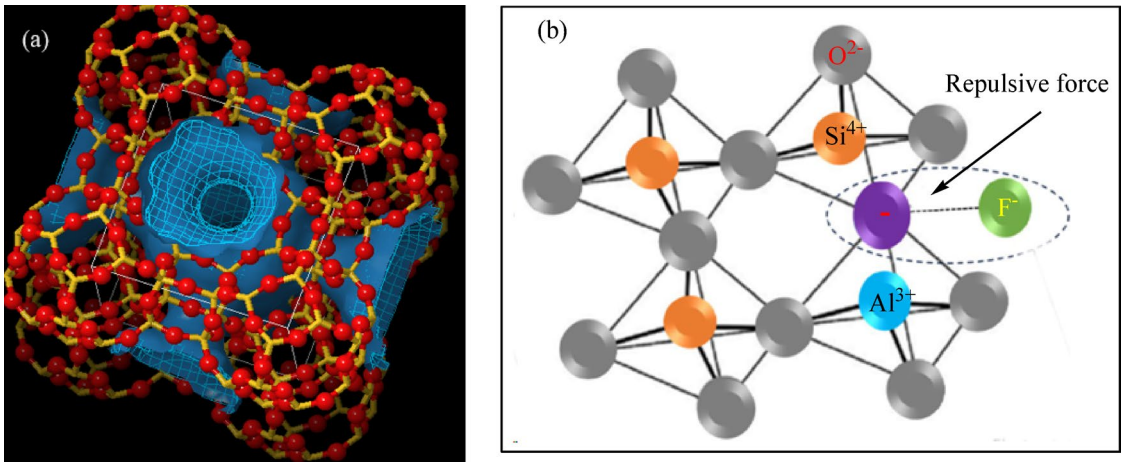

Fig. 1. Porosity of Z-A (**a**), and electrostatic repulsion between zeolite surface charge and fluoride (**b**) drawn by Adobe Photoshop [19].

(98%, *UDYOG, India),* $C_2H_4O_2$ (99.8%, *Pentokey Organy, India*), and NaF (99%, *Sigma-Aldrich*) were obtain from central laboratory, AASTU, Ethiopia. The corn (source of corn cob) was purchased from a street market in Addis Ababa city, Ethiopia. Furthermore, kaolin was collected from western Homa near Hossana, Ethiopia, which was used as raw material for the synthesis of Z-A. Groundwater sample was collected from Kenteri town, Bora woreda, Ethiopia.

Instruments

The phase structural and crystallinity of the synthesized adsorbent was examined by X-Ray Diffraction Spectroscopy (XRD, *Bruker-AXS D8, Advance Type,) at* Cu kα radiation (λ = 1.54 A°, 40 kV, 44 mA). The functional groups were analyzed using Transform-Infrared Spectroscopy (*FT-IR, iS50 ABX, Germany*). The surface area of synthesized adsorbent was scrutinized using Brunauer–Emmett–Teller (BET, *Quantachrome AUTOSORB-1, USA*). The surface morphology and elemental composition of synthesized adsorbent were also characterized by Scanning Electron Microscopy coupled with energy dispersive spectroscopy (*SEM–EDS, JEOL JSM-6500F,* Japan). The concentration of fluoride was measured using fluoride ion selective electrode (*Metrhom-6.0502.150, Germany*).

Adsorbent synthesis

Synthesis of magnetite (Fe_3O_4)

The Fe_3O_4 was synthesized through the co-precipitation method[23] at a 2:1 molar ratio of $FeCl_3 0.6H_2O$ to $FeCl_2 0.4H_2O$ using as a precursor and NaOH as a precipitating agent. To describe briefly: 4 g of $FeCl_2 0.4H_2O$ and 8 g of $FeCl_3 0.6H_2O$ were dissolved in 180 mL of distilled water and stirred for 2 h at 70 °C. The 4 M NaOH solution was added dropwise into the solution till the pH reached 10[19,24]. The solution was allowed for 12 h to precipitate at room temperature. The precipitate was separated via magnetic bar and washed with distilled water and acetone[16,19]. Hereafter, the precipitate was oven-dried at 60 °C for 6 h.

Synthesis of BC and M-BC composite

Initially, the BC was synthesized through pyrolysis of corn cobs according to the procedure[25,26] with a little bit of modification. The corn cob was dried and crushed into powder. 5 g of powder was pyrolyzed in a muffle furnace at 450 °C for 3 h under a 5 °C min^{-1} N_2 gas flow rate[27]. Afterward, the BC was ground and sieved using 100 mm Mesh sieve. Secondly, the BC was magnetized by dispersing 10 g of BC in 200 mL of distilled water with continuous stirring for 30 min[28]. In another beaker, 7 g of $FeSO_4 0.7H_2O$ and 14 g of $FeCl_3 0.6H_2O$ were dissolved in 100 mL of distilled water and stirred for 1 h at 60 °C. This solution was transferred into BC suspension and stirred for another 1 h at 60 °C. Then, 4 M of NaOH solution was added dropwise at ambient temperature to adjust the pH to 10[24]. Then, the solution was allowed 12 h to co-precipitate. The precipitate was collected by magnetic bar and dried for 12 h at 60 °C.

Synthesize of Z-A

Z-A was synthesized through the hydrothermal method according to the procedure reported previously[17,19]. To describe briefly: 40 g of raw kaolin was soaked with 400 mL of distilled water for 4 days with continuous stirring. The suspension was centrifuged and dried. The treated kaolinite was calcined at 700 °C for 3 h. Fine powder metakaolin was treated with 4 M NaOH-hot water (1:5 m/v ratio) and heated in a water bath for 1 h at 70 °C for gel formation (Scheme 1). The gel was aged for 12 h at room temperature and heated at 110 °C for 12 h in a Teflon-lined steel autoclave. The product was centrifuged, washed many times with deionized water, and dried in an oven at 80 °C.

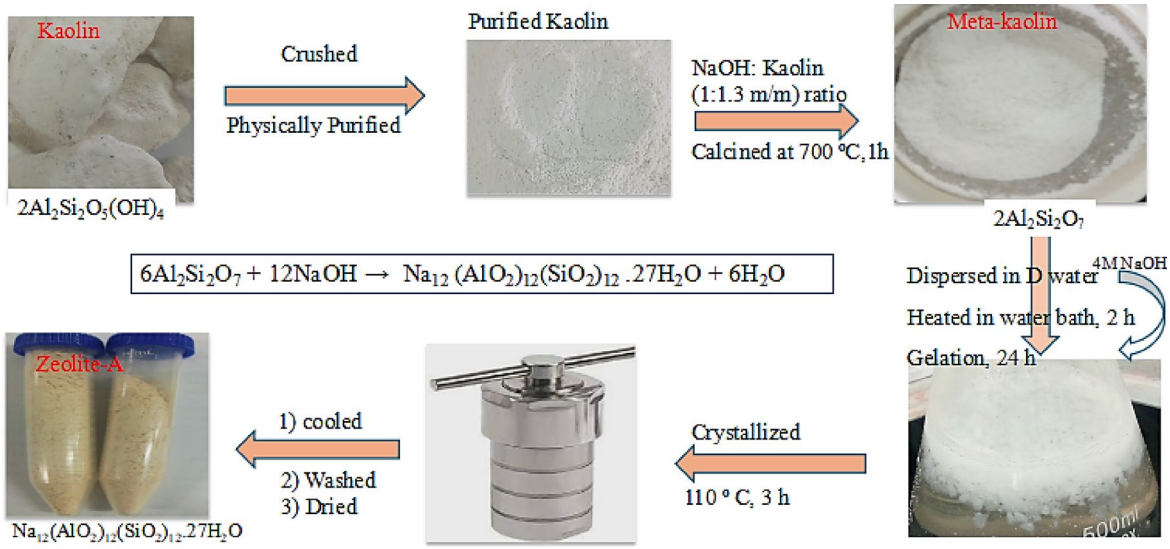

Scheme 1. Synthesis of Z-A through hydrothermal method.

Synthesis of Z-A/M-BC composite

Z-A/M-BC composite was synthesized by the pyrolysis method[17,29]. Typically: 3.6 g of Z-A and 7.2 g of M-BC were dispersed in 150 mL of deionized water[30]. The mixture was stirred for 3 h and allowed to react at ambient temperature for 24 h. The suspension was centrifuged and dried at 80 ℃ in an oven for 6 h[16]. The dried solid was pyrolyzed (5 °C/min) at 450 ℃ for 3 h[31]. The crucible was desiccated and the resulting composite material was ground.

Adsorption studies

Determination of zero-point charge (pH_{zpc})

The zero-point charge of Z-A/M-BC absorbent was investigated at 3, 5, 7, 9, and 11 pH using 05 M HCl and 0.05 M NaOH[19,32]. 1.5 g of the synthesized adsorbent was added into each 50 mL of the pre-pH adjusted solution. The solution was shaken for 90 min using an orbital shaker and allowed for 20 h. Hereafter, the adsorbent was separated by an external magnetic bar and the pH values of each filtrate were recorded. The pH_{ZPC} of the adsorbents was identified from a common intersection point of the curve of initial pH and their corresponding ΔpH change[33].

Parameters optimization

Firstly, ionic strength adjustment buffer type I (TISAB-I) was prepared according to the procedures reported by Gao et al. and Teju et al.[6,10,19]. To describe briefly: 58 g of NaCl and 7 g of $Na_3C_6H_5OH.nH_2O$ were dissolved in 500 mL distilled water. And then 57 mL CH_3COOH was added to the solution. The pH of solution was maintained to 5.3 using 0.5 M NaOH. The standard solutions (2, 4, 6, 10, and 14 mg/L) were also prepared through serial dilution from the stock solution for sketching of the calibration curve (Fig. S1). Then after, the removal study was commenced by optimizing the removal parameters such as pH, adsorbent dose, C_o, and contact time[3,15,34].

The impact of pH on the removal test was studied at pH values of 3, 5, 7, 9, 11, and 13 using 0.05 M HCl and 0.05 M NaOH solutions at 1.5 g/L of adsorbent dose, 10 mg/L of C_o, and 6 h of contact time[33]. The effect of C_o was examined at 5, 10, 15, 20, 30, and 40 mg/L[8] (contact time = 6 h, pH = 5, adsorbent dose = 1.5 g/L). The effect of adsorbent dose on fluoride removal efficiency was studied at adsorbent doses of 0.5, 1, 1.5, 2, and 2.5 g/L (C_o = 10 mg/L, contact time = 6 h, pH = 5). The impact of contact time was also studied by varying the adsorption time from 3 to 15 h (3, 6, 9, 12, 15 h) at a pH of 5, 1.5 g/L of adsorbent dose, and 10 mg/L of C_o. The mixture was shaken at 160 rpm for 90 min, equilibrated for 6 h, and then separated by an external magnet. After a while, 10 mL of TISAB was added to a polyethene bottle containing 20 mL filtrate, and the removal test was measured using FISE[13,19]. A real water sample analysis was also carried out by taking groundwater having 12.25 mg/L an C_o from Kenteri town, Bora Woreda, Ethiopia, at confined conditions. The removal capacity (Qe), and efficiency (R) were evaluated using Eqs. (1) and (2), respectively[8,19].

$$Q_e = \frac{(C_o - C_e)\,V}{W} \tag{1}$$

$$\%R = \frac{(C_o - C_e)}{C_o} \times 100\% \tag{2}$$

Where, C_0 and C_e represent the initial and equilibrium fluoride concentration (mg/L), respectively, V (mL) is the volume of solution, W (g) is the amount of the adsorbent.

Reusability test

The reusability of Z-A/M-BC was commenced by dispersing of fluoride exhausted adsorbent in 50 mL of 0.05 M NaOH solution and was shaken using an orbital shaker at 160 rpm for 90 min for desorption of fluoride[19,35]. The adsorbent was separated and an oven dried at 60 °C overnight. Thereafter, the activated Z-A/M-BC was reused for five successive removal tests at optimum conditions (contact time = 6 h, pH = 5, adsorbent dose = 1.5 g/L, C_o = 10 mg/L).

Results and discussion

Characterization of adsorbents

PXRD analysis

The PXRD peak in the range of 2θ = 10–30° was observed, which confirms the formation of amorphous BC (Fig. 2a). The PXRD peaks for Fe_3O_4 at 2θ = 30.33°, 35.53°, 43.42°, 57.08°, and 63.02° corresponded to (220), (311), (440), (511), and (440) the lattice planes, respectively (Fig. 2a). This result closely coincided with PXRD data reported by[19,36] and verified the formation of Fe_3O_4. The broad peak from 20–30° and at 18.36°(111), 30.33°(220), 35.47°(311), 43.02(400), 57.14°(511), and 62.59°(440) indicate the coexistence of Fe_3O_4 and BC in the M-BC composite (Fig. 2a); the peak location of Fe_3O_4 did not alter after loading of Fe_3O_4 onto BC[19,29]. Besides, the presence of new peaks at 7.16°, 10.16°, 13.92°, and 21.71° suggests the formation of new interactions between Fe_3O_4 and BC in the M-BC composite[17,19]. The existence of a peak at 2θ = 30° indicated the existence of Z-A, which played a major role in the Z-A/M-BC composite formation[16]. Besides, the PXRD peaks of Fe_3O_4 and M-BC also appeared in their composite Z-A/M-BC composite, demonstrating the co-occurrence of Z-A and M-BC in the Z-A/M-BC composite material (Fig. 2b). Additionally, the occurrence of an intensified peak at 23.72° indicated the strong interaction between Z-A and M-BC, while the presence of new peaks at 69.10° and 77.42° suggested the formation of new bonds between Z-A and M-BC in the Z-A/M-BC adsorbent[37].

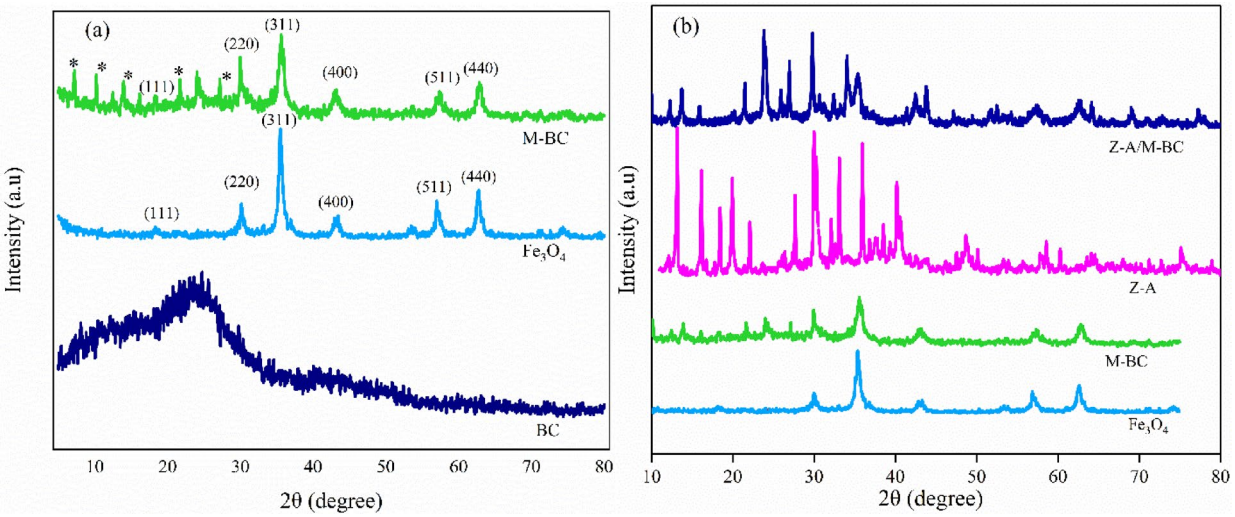

Fig. 2. PXRD results of synthesized adsorbents.

The average particle size of the Z-A/M-BC composite was s estimated[19,38] using Scherer's Equation (3) and found to be 27.98 nm. The BET result also indicates the porous nature of the synthesized Z-A/M-BC adsorbent with 496.17 m^2/g surface area and 0.08936 cm^3/g pore volume (Fig. S2 and Table S1).

$$D = \frac{k\lambda}{\beta \cos\theta} \tag{3}$$

where D is the crystallites' size, k is Scherer's constant depending on the shape of particles (0.94), λ wavelength of the X-ray radiation (0.15418 nm for CuKα), β is the full width of half maximum (FWHM) intensity (in degree which converted to radian), and θ is the diffraction (Bragg) angle.

FT-IR analysis

The representative peak of BC at 3209 cm^{-1} corresponded to the -OH stretching vibration, which is ascribed to water molecules[39]. Peaks at 3040 and 2912 cm^{-1} are attributed to stretching variations of = C-H and -C-H (Fig. S3a), respectively[17,27]. Peaks at 1574 and 1157 cm^{-1} correspond to C = C stretching variations in aromatic groups and C-O stretching vibration, sequentially[37]. Peaks at 871, 805, and 750 cm^{-1} reveal the existence of inorganic impurities (Si–O/Fe–O bonds), which are already shown in the EDX result (Fig. 4a). Peaks at 971 and 781 cm^{-1} are attributed to the symmetric and asymmetric vibration bands of the TO_4 tetrahedron (Fig. S3b) (where T = Si or Al), respectively[16]. Wavenumbers at 542 and 458 cm^{-1} are attributed to asymmetric external and symmetric internal vibrations of the double ring of Si and Al TO_4[17,40]. Wavenumbers around 3400 and at 1648 cm^{-1} suggested the stretching and bending vibration of H_2O molecules in the Z-A framework, respectively[41].

The FT-IR peaks at 430, 538, 794, and 889 cm^{-1} are attributed to Fe–O bond formation in Fe_3O_4. Wavenumbers at 1629 and 3367 cm^{-1} also signify the bending and stretching vibration of the -OH on the surface of Fe_3O_4 sequentially (Fig. S3c). The FT-IR peak at 580 cm^{-1} (Fe–O) in the M-BC composite also confirmed the presence of Fe_3O_4 in the modified M-BC composite[36]. Attenuation of -OH intensity in the M-BC composite (Fig. S3d) proved the importance of hydrogen bonding in M-BC composite formation[29]. The prominent peak of Z-A/M-BC at 1438 cm^{-1} is ascribed to the symmetric stretching vibration of the carboxylate ion. Peaks around 3357 and at 1638 cm^{-1} corresponded to the stretching and bending vibration of O–H sequentially. The peak at 2359 cm^{-1} is associated with the C-O stretching vibration[42]. Peaks at 972, 553, and 488 cm^{-1} reveal the presence of M–O bonds (M = Si, Fe, Al) (Fig. S3d).

SEM analysis

The SEM images of synthesized adsorbents were shown in Fig. 3a–d. The SEM result of Z-A revealed the presence of a cubic crystal structure with a size in the 0.565–4.25 µm range (Fig. 3a). The SEM image of pristine BC is noticed to be rough and irregular with average sizes of 8.74 µm (Fig. 3b). The SEM image of the M-BC composite shows them stuck to each other because of the presence of large surface energy[40] and spherical-shaped particles of Fe_3O_4 (Fig. 3c). The average size of M-BC was found to be 0.47 µm. The SEM image of Z-A/M-BC (Fig. 3d) is observed as nearly spherical with an average size of 0.098 µm[43].

EDX results

The EDX band of pristine BC contains the anticipated elements of C and O, which are the main components of a distinctive BC material (Fig. 4a). The %weight of elemental composition of Z-A is found to be 20.84% Si, 17.46% Al, 48.58% O, and 12.85% Na, which confirms the purity of the synthesized material (Fig. 4b). As anticipated, the ratio of Si/Al for the as-synthesized Z-A was found to be 1.19, which is close to 1. This is further used to support the formation of pure Z-A[19]. The M-BC adsorbent encompasses 52.28% C, 22.07% O, 4.78% Al, 5.90% Si, 1.97%

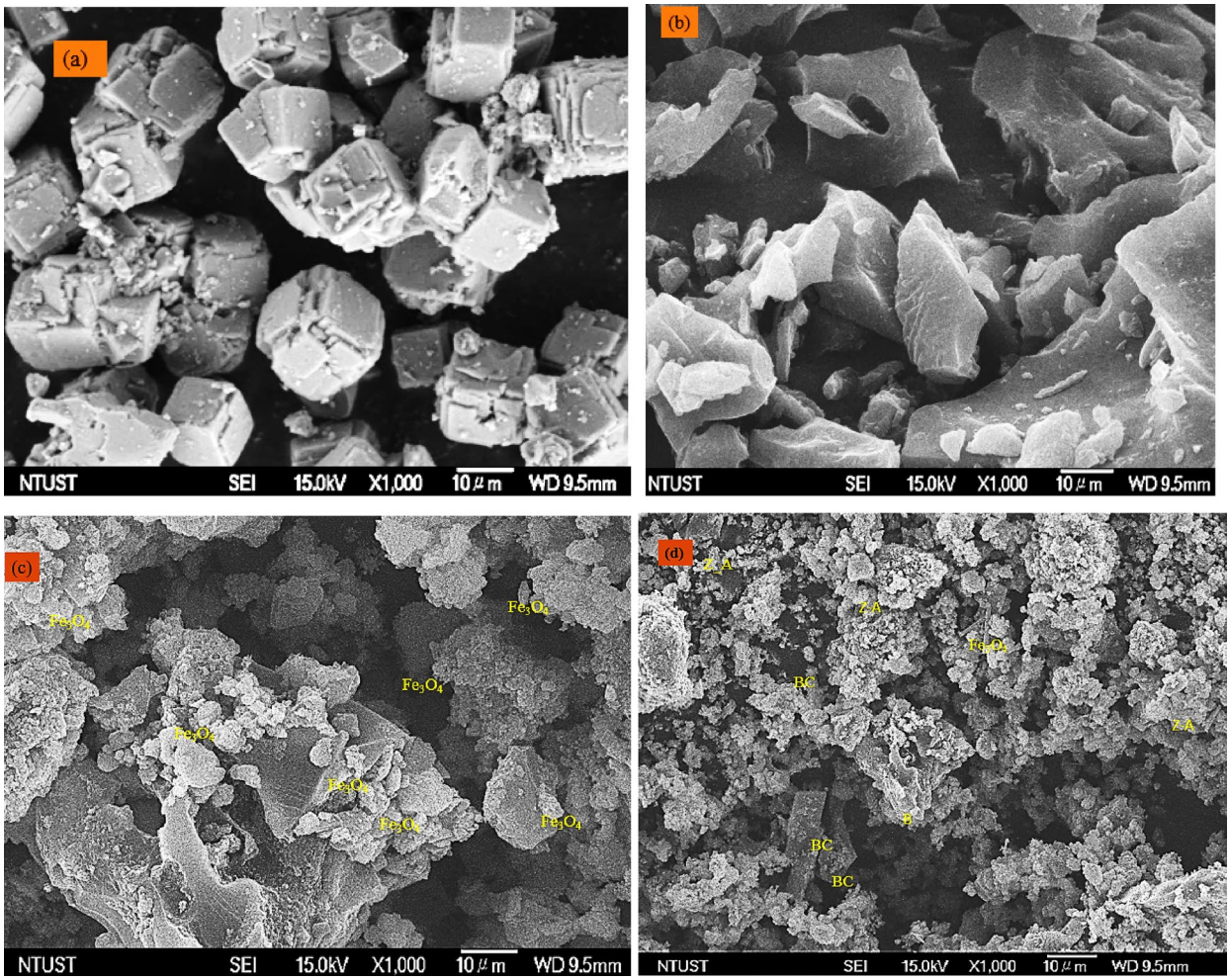

Fig. 3. SEM images of Z-A (**a**), BC (**b**), M-BC (**c**) and Z-A/M-BC (**d**).

Ca, and 12.49% Fe[17] as it demonstrated in Fig. 4c. The anticipated elemental compositions of the Z-A/M-BC composite were found to be 47.25% C, 31.55% O, 3.03% Na, 2.62% Al, 3.65% Si, and 11.88% Fe (Fig. 4d). The elemental mapping distribution of synthesized adsorbents was illustrated in Fig. S4.

Adsorption study

Determination of zero-point charge

In this work, the surface zero-point charge of Z-A/M-BC is determined and found to be 6.75 (Fig. 5). In this regard, when the solution pH is less than the pHZPC values, the net surface charge of the synthesized adsorbent becomes protonated and positively charged, having a greater attraction with fluoride. When the pH is above the PZC value, the surface of synthesized adsorbents is deprotonated (hydroxyl groups developed), which results in low removal capacity owing to their electrostatic repulsion force[17,19].

Adsorption factors

The impact of pH on fluoride removal efficiency was investigated at different pH values (3, 5, 7, 9, 11, and 13) and resulted in 90.20%, 89.90%, 81.30%, 64.50%, 54.10%, and 51.10%, respectively (Fig. 6a). The highest removal efficiency was obtained at pH of 3 and 5, respectively. However, pH 3 is inadequate for the practical removal of fluoride from groundwater. To offset this, all fluoride removal tests were conducted nearly neutral (pH = 5). After a while, the removal efficiency is decreased due to competition between OH^- and fluoride ions for adsorption sites and coulombic repulsion force. The removal efficiency of Z-A/M-BC was found to be 75.00%, 88.91%, 91.50%, 93.80%, and 94.40% at 0.5, 1.0, 1.5, 2, and 2.5 g/L adsorbent doses (Fig. 6b), respectively, which increased with adsorbent dose. This is possibly due to the increment of free active sites on the adsorbent surface[1,9]. Nevertheless, the removal efficiency shows a negligible increment after 1.5 g/L; this may be due to the saturation of adsorbent sites[9].

The influence of C_o on the removal efficiency of Z-A/M-BC was executed at 5, 10, 15, 20, 30, and 40 mg/L and resulted in 83.60%, 92.80%, 90.53%, 78.75%, and 67.63%, respectively (Fig. 6c). The maximum adsorption efficiency (92.20%) was attained at 10 mg/L C_o of fluoride. However, exceeding 10 mg/L, the removal efficiency decreased. This may be due to the competition among adsorbates for fixed active sites of the synthesized

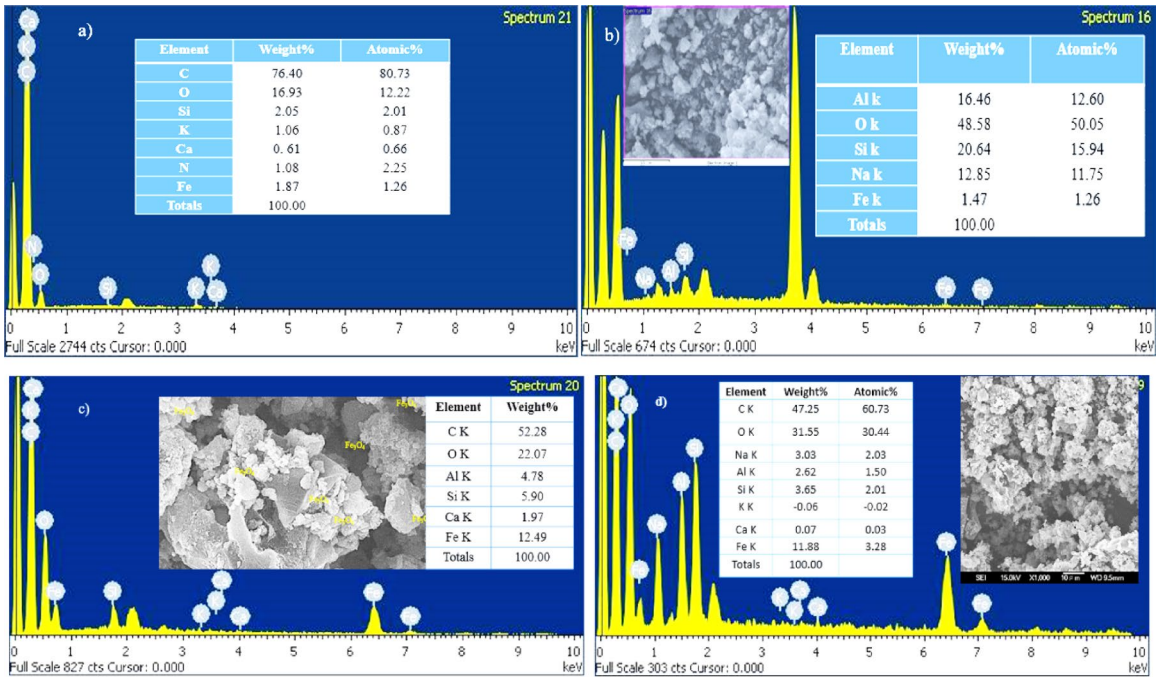

Fig. 4. Elemental analysis of BC (**a**), Z-A (**b**), M-BC (**c**), and Z-A/M-BC (**d**).

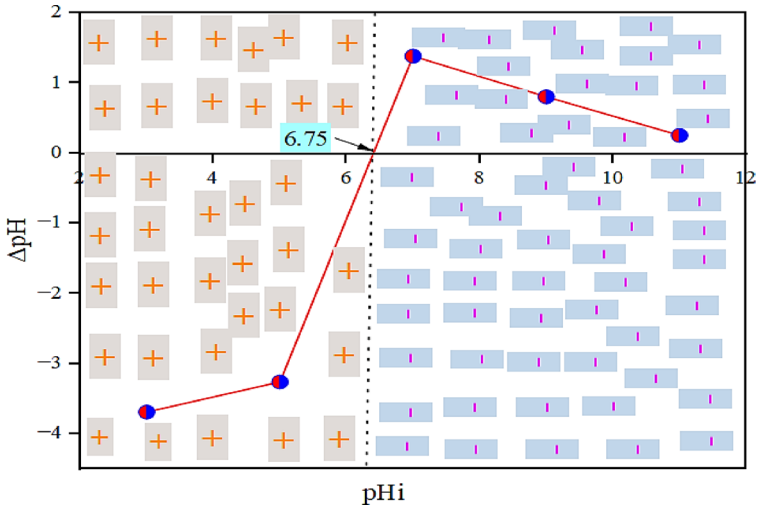

Fig. 5. Zero-point charge of Z-A/M-BC composite.

adsorbent[19]. The removal efficiency of Z-A/M-BC was found to be 80.30%, 92.20%, 93.10%, 93.80%, and 95.60% at contact time of 3, 6, 9, 12, and 15 h, respectively (Fig. 6d). The adsorption efficiency shows a slow increment after the optimum adsorption time (6 h). Consequently, the adsorption efficiency of synthesized increased contact time[1,4,15].

Adsorption isotherms

The adsorption isotherm is used to indicate whether the adsorbent surface is homogeneous or heterogeneous in which the adsorbate molecules are distributed over the surface[1]. The adsorption isotherm was tested using the Langmuir and Freundlich isotherms (Fig. 7). The linear form of Langmuir and Freundlich isothermal models were displayed using Eqs. (4) and (5), respectively[18,35].

$$\frac{\mathrm{Ce}}{\mathrm{Qe}} = \frac{1}{\mathrm{K}_L \mathrm{Qm}} + \frac{\mathrm{Ce}}{Qm} \tag{4}$$

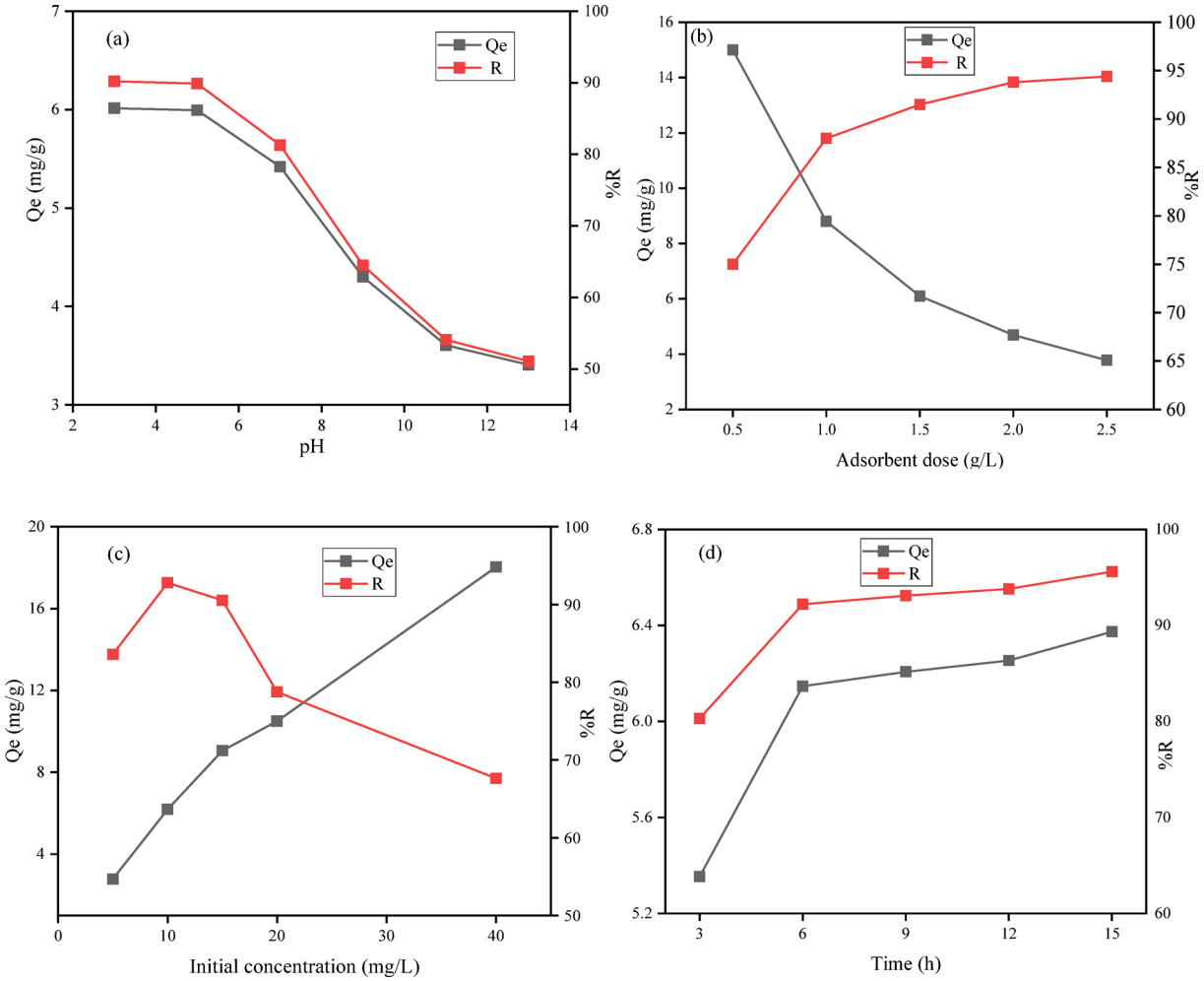

Fig. 6. Impacts of (**a**) pH, (**b**) adsorbent dose, C_o (**c**), and contact time (**d**) on removal efficiency and capacity of Z-A/M-BC composite.

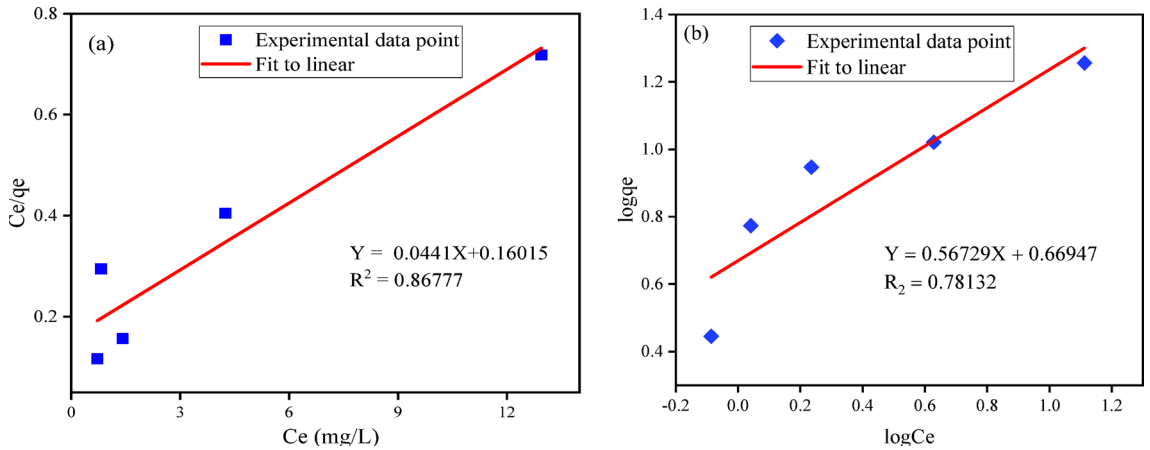

Fig. 7. Langmuir adsorption isotherm model (**a**), and Freundlich adsorption isotherm model (**b**).

$$\log Q_e = \log K_F + \frac{1}{n} \log C_e \tag{5}$$

where C_e is the equilibrium concentration of F^- in the solution (mg/L); Q_e is the amount of fluoride adsorbed per unit weight of Z-A/M-BC (mg/g), Q_m is the maximum adsorption capacity (mg/g) and K_L is the Langmuir constant related to energy (L/mg), K_F and n are dimensionless constants which are relative adsorption capacity and intensity of adsorption, respectively.

The values of Qm and KL of the linear expression of the Langmuir adsorption isotherm were calculated from the slope and intercept of the linear plot of Ce versus Ce/Qe. The small values of KL (0.2754 L/mg) indicate the weak interaction of adsorbate with the Z-A/M-/BC surface. Besides, the low value of (R^2 = 0.86777) doesn't explain the defluoridation activities adequately. In the Freundlich adsorption isotherm, the values of 1/n (0.4829) lying between 0.1 and 1.0 and n (2.071) lying in 10 > n > 1 (Table S2) imply that the adsorption of fluoride on the Z-A/M-BC surface is privileged. Nevertheless, the values of KF and R^2 were found to be 5.416 mg/g and 0.6334, respectively[35], which is far from the model. Unfortunately, neither the Langmuir nor the Freundlich isotherm model was well fit to express the defluoridation activities.

Kinetic models

The pseudo-first-order and pseudo-second-order use to familiar with the adsorption mechanisms and adsorption rate[44]. The fitness of pseudo-first order and pseudo-second order were evaluated using Eqs. (6) and (7), respectively.

$$\text{pseudo - first order} \ : \log(Qe - Qt) = \log Qe - \frac{K_1 t}{2.303} \tag{6}$$

$$\text{pseudo - second order} \ : \frac{t}{Qt} = \frac{1}{mK_2 Qe} + \frac{t}{Qe} \tag{7}$$

where Q_e is the amount of fluoride adsorbed per unit weight of Z-A/M-BC at equilibrium (mg/g), Q_t is the amount of fluoride adsorbed per unit weight of Z-A/M-BC (mg/g) at time t (min), and k_1 and k_2 is the first and second pseudo-order rate constant for the adsorption (min^{-1}), respectively.

The sketch of log (Qe-Qt) against time (Fig. 8a) gives a linear relationship of the pseudo-first-order rate. The correlation factor (R^2) of both pseudo-first-order (0.9515) and pseudo-second-order kinetics (0.999) are fitted (Table S3). However, the pseudo-first-order model is not appropriate to describe the adsorption kinetics since the theoretical adsorption capacity (Qm fit = 4.44 mg/g) was far from the experimental value (Qm exp. = 6.147 mg/g). On the other side, the linear plot of t/Qt versus time shows a higher coefficient (R^2 = 0.999) for the pseudo-second-order kinetic model (Fig. 8b). Furthermore, the theoretical adsorption capacity (Qm fit = 6.62 mg/g) was closer to the experimental adsorption capacity (Qm exp. = 6.147 mg/g). Thus, the adsorption process best obeys the pseudo-second-order kinetic model in which the removal of fluoride is primarily controlled by chemisorption processes such as chemical precipitation, hydrogen bonding, ion exchange, and electrostatics[17,19].

Response surface method (RSM) study

The mutual interaction impacts of defluoridation parameters (contact time, C_o, and adsorbent dose) were also detected (at 17 runs) using the Box-Behnken model (Table S4) at constant pH = 5 Hereafter, the response and the input variables are expressed using a quadratic model-coded Eq. (8).

$$\begin{aligned} \%R = {} & 86.57 + 1.924\mathrm{A} - 3.35\mathrm{B} + 1.20\mathrm{C} + 1.06\mathrm{AB} + 860\mathrm{AC} \\ & + 0.1550\mathrm{BC} - 0.625\mathrm{A}^2 - 0.3125\mathrm{B}^2 + 0.2475\mathrm{C}^2 \end{aligned} \tag{8}$$

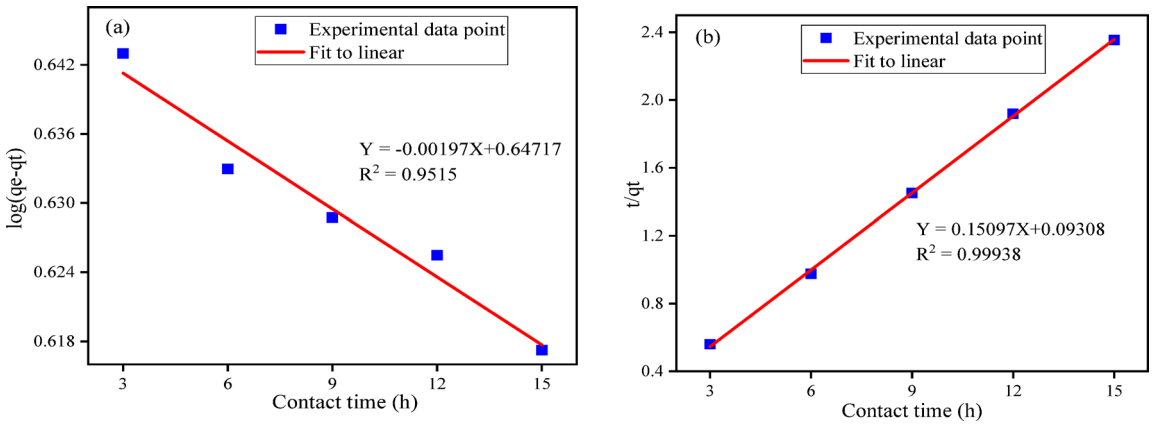

Fig. 8. Pseudo-first-order kinetics model (**a**), and pseudo-second-order kinetics model (**b**).

where A, B, and C are the coded values of the operation variables for adsorbent dose, C_o, and contact time, respectively.

The model fitness was checked based on the values of the coefficient of determination (R^2). The proximity of R^2 value to unity (R^2 = 0.9973), and the intimacy of adjusted (R^2 adj = 0.9939) and predicted R^2 (R^2 pred = 0.9574) values to each other with the difference < 0.2 suggest the fitness of model[17]. The predicted R^2 value is reasonably agreed with the adjusted R^2 value, which approves the model's fitness (Table S5). Besides, the precision that measures the signal-to-noise ratio (AP = 65.34) is greater than 4; indicating a good signal and accurate model fit[17]. The F-value of 291.61 suggests that the model is significant. The P-values < 0.0500 indicate the significance of the model. In this regard, A, B, C, AB, AC, and A^2 are significant (Table S5). Consequently, the Box-Behnken model was verified and statistically proved to be reliable and adequate in defluoridation of drinking water.

The mutual impacts of contact time and C_o exhibited a positive effect on the defluoridation efficiency (Fig. 9). But individually, the C_o showed negative effects whereas the contact time showed a positive impact on the removal of fluoride[17]. The mutual interaction impacts of Z-A/M-BC dose and contact time on the removal of fluoride showed positive effects (Fig. 10). The collaboration of adsorbent dose and C_o of fluoride (Fig. 11) also shows favorable effect on the removal of fluoride.

Real sample analysis and reusability test

Before applying the removal test, the content of anions in the groundwater (Cl^-, NO_3^-, CO_3^{2-}, SO_4^{2-}, and PO_4^{3-}) was analyzed[19,44] and the results were tabulated in Table S6. Then the performance of the as-synthesized adsorbent was applied for defluoridation of a real water sample having 12.25 mg/L C_o, which was collected from Kenteri town, Ethiopia. The equilibrium concentration of fluoride was reduced to 1.35 mg/L (Table S6), which meets the acceptable limit of fluoride concentration in potable water endorsed by WHO[19]. The removal efficiency of synthesized adsorbents (Z-A, BC, M-BC, and Z-A/M-BC) was found to be 46.45%, 51.82%, 44%, and 88.97%, respectively (Fig. 12a). The Z-A/M-BC composite relatively shows better removal efficiency than its pristine materials. However, the Z-A/M-BC composite shows relatively lower removal efficiency in a real water sample than in a simulated water sample. This could be due to the presence of different matrix ions in groundwater (Table S6). The economic viability of the as-synthesized adsorbents was checked by the reusability test. The reusability test of the synthesized Z-A/M-BC composite was found to be 95.80%, 90.40%, 87.30%, 85.40%, and 70.20% removal efficiency for the first, second, third, fourth, and fifth cycles, respectively, which is almost constant removal efficiency from the first to fourth cycles (Fig. 12b).

Comparison of Z-A/M-BC removal efficiency with previous reports

The fluoride removal efficiency of Z-A/M-BC was compared with other adsorbents which was reported previously (Table 1). Accordingly, the synthesized adsorbent shows good defluoridation efficiency. Thus, the finding of this research work suggests that the Z-A/M-BC is a good adsorbent for the defluoridation groundwater.

Adsorption mechanisms

The removal mechanism of fluoride via Z-A/M-BC involves surface complexation/precipitation, ion exchange, hydrogen bonding, and electrostatic interaction (Fig. 13). The hydroxyl groups (M-OH) are substituted by fluoride, and the removal of fluoride proceeds through anion exchange[19]. The defluoridation of fluoride also proceeds via a complexation/precipitation mechanism; fluoride is a hard base that is highly affinized to hard acids (Al^{3+}, Fe^3, and Si^{4+}) to form stable products. Most importantly, the defluoridation mechanism occurred via electrostatic interaction on the basis of PZC.

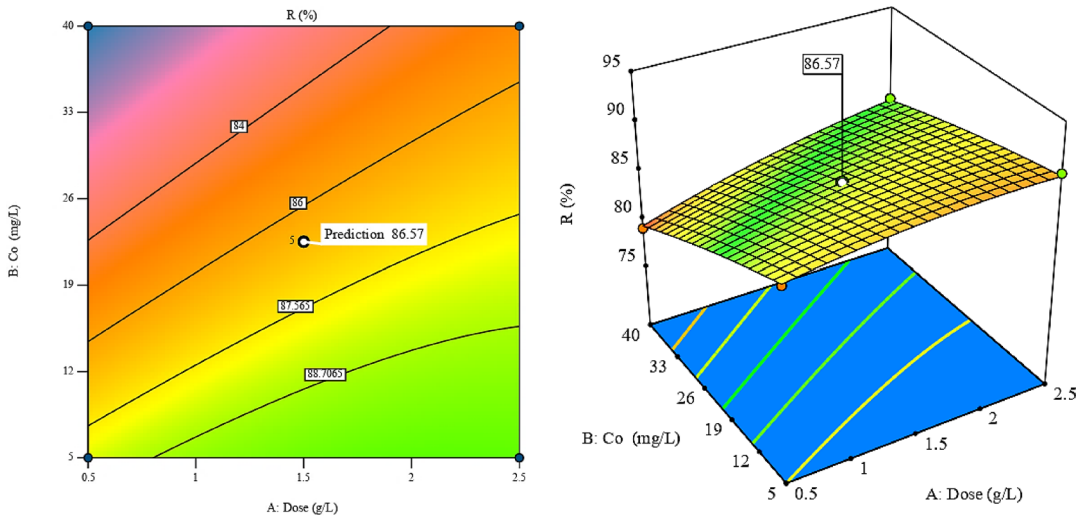

Fig. 9. Two-dimensional and three-dimensional surface plots showing the C_o and adsorbent dose on the removal of fluoride by Z-A/M-BC composite.

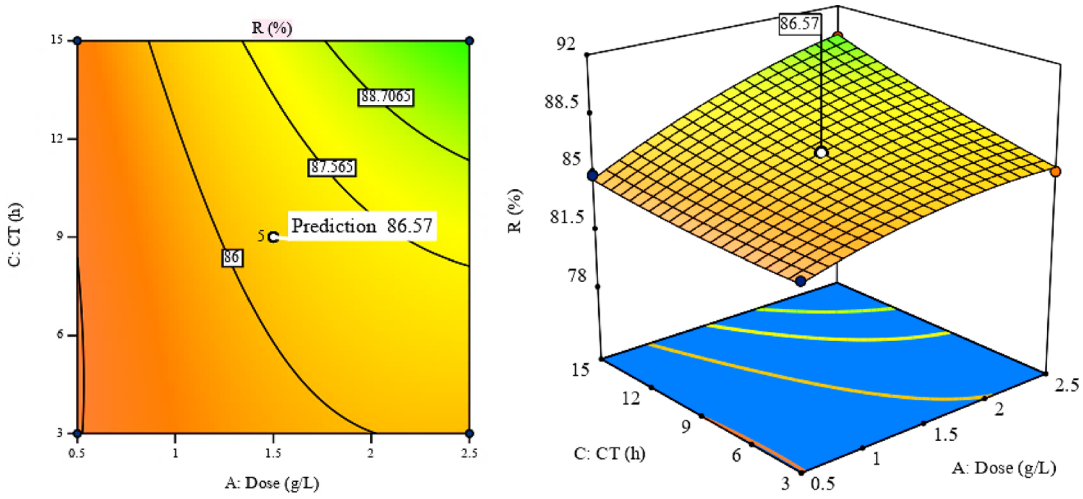

Fig. 10. Two-dimensional and three-dimensional surface plots showing the effect of adsorbent dose and contact time on the removal of fluoride by Z-A/M-BC composite.

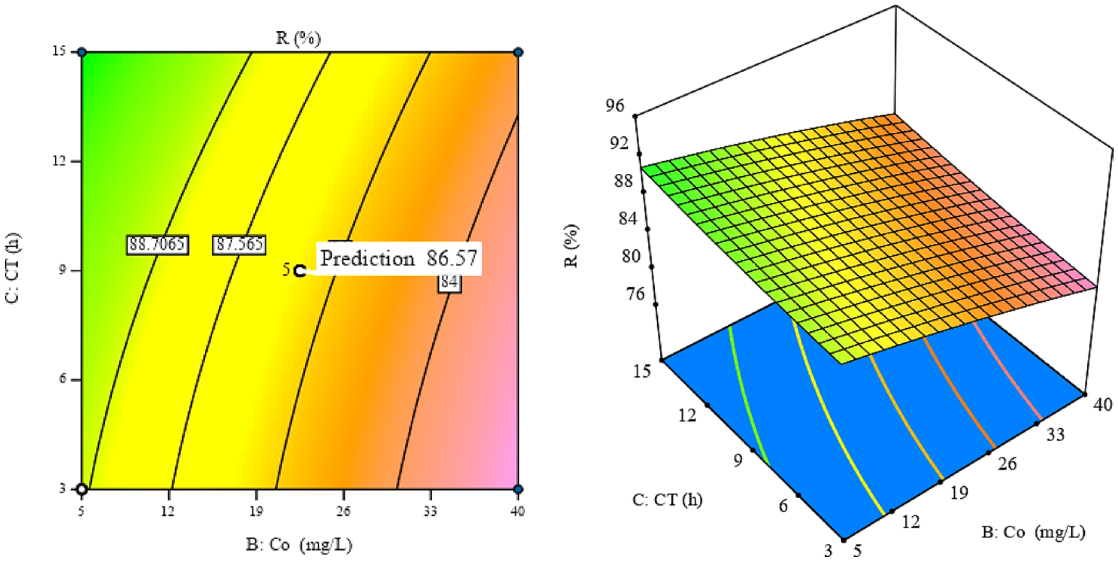

Fig. 11. Two-dimensional and three-dimensional surface plots showing the impact of C_o and contact time on the removal of fluoride by Z-A/M-BC composite.

Conclusions

In the present work, Z-A/M-BC adsorbent was synthesized for the removal of fluoride groundwater. The crystalline size, functional groups, surface area, elemental composition, and morphology of the synthesized Z-A/M-BC composite were also characterized by using PXRD, FT-IR, BET, and SEM–EDX to confirm the formation of adsorbent material. The removal efficiency of Z-A/M-BC adsorbent was started by optimizing pH, adsorbent dose, C_o, and contact time. The maximum removal efficiency (95.80%) and capacity (6.37 mg/g) were obtained at pH 5, an adsorbent dose of 1.5 g/L, a contact time of 6 h, and C_o of 10 mg/L. Furthermore, the reusability study was found to be 95.80%, 90.40%, 87.30%, 85.40%, and 70.20% removal efficiency for the first, second, third, fourth, and fifth turns, respectively. This suggests that the Z-A/M-BC composite is efficient and can be reused for the removal of groundwater. The as-synthesized adsorbent was also applied for the defluoridation of a real water sample having 12.25 mg/L fluoride Co, which was reduced to 1.35 mg/L, which meets the permissible limit of fluoride concentration in drinking water recommended by WHO. Thus, the synthesized adsorbent is useful for the removal of fluoride from groundwater.

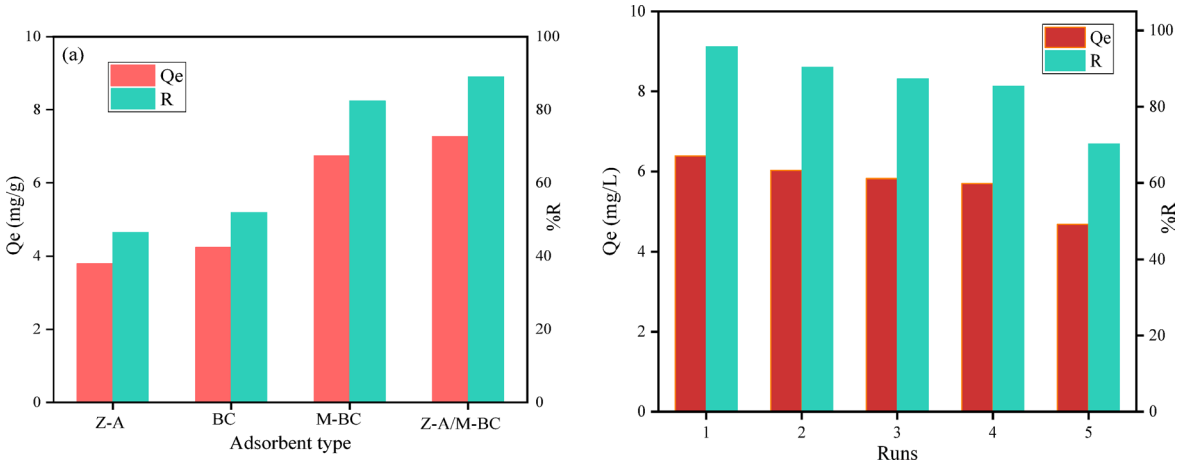

Fig. 12. Effects of adsorbent nature on the removal efficiency and capacity of Z-A/M-BC (**a**), and reusability (**b**).

S. no	Adsorbents	Removal efficiency (%)	Refs.
1	Fe_3O_4/graphene/alginate nanocomposite	85.50	38
2	Lanthanum-doped—activated carbon (AC-La),	92.00	2
3	Zirconia/Zeolite (ZrO_2-Ze)	94.89	10
4	Activated carbon of *Catha edulis*	73.00	8
5	Zirconium-MOF (MOF-801)	95.20	16
6	Aluminum hydroxide-loaded zeolite	92.00	3
7	Z-A/M-BC	95.80	This study

Table 1. Comparison of the defluoridation efficiency of Z-A/M-BC composite with previous reports.

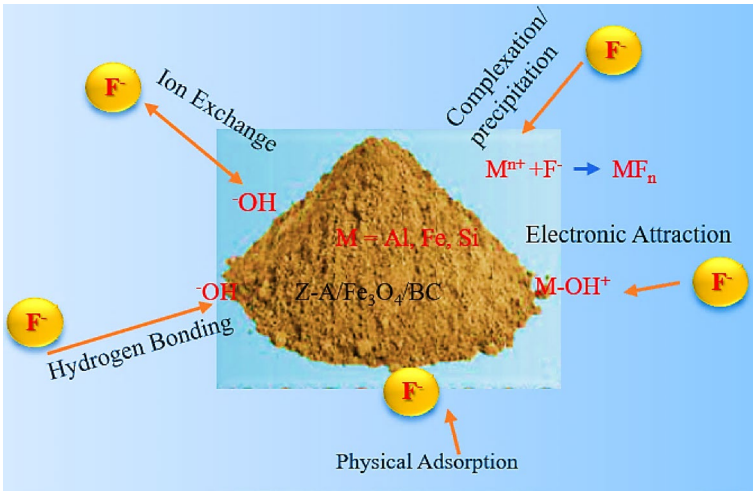

Fig. 13. Proposed removal mechanism of fluoride via Z-A/M-BC composite.

Data availability

Data available upon request from the corresponding author.

Received: 24 October 2025; Accepted: 2 December 2025
Published online: 20 January 2026

References

1. Gómez-Hortigüela, L., Pérez-Pariente, J., García, R., Chebude, Y. & Díaz, I. Natural zeolites from Ethiopia for elimination of fluoride from drinking water. *Sep. Purif. Technol.* **120**, 224–229. https://doi.org/10.1016/j.seppur.2013.10.006 (2013).
2. Zhang, Y. et al. Defluorination and regeneration study of lanthanum-doped sewage sludge-based activated carbon. *J. Environ. Chem. Eng.* **9**, 105740. https://doi.org/10.1016/j.jece.2021.105740 (2021).
3. Chen, J., Yang, R., Zhang, Z. & Wu, D. Removal of fluoride from water using aluminum hydroxide-loaded zeolite synthesized from coal fly ash. *J. Hazard Mater.* **421**, 126817. https://doi.org/10.1016/j.jhazmat.2021.126817 (2022).
4. Dhillon, A., Soni, S. K. & Kumar, D. Enhanced fluoride removal performance by Ce–Zn binary metal oxide: Adsorption characteristics and mechanism. *J. Fluor. Chem.* **199**, 67–76. https://doi.org/10.1016/j.jfluchem.2017.05.002 (2017).
5. Raghav, S., Sapna, & Kumar, D. Cubical-shaped rods of pectin-hydroxyapatite composite for adsorption studies of fluoride by statistical method and adsorption experiments. *ACS Omega* **3**, 9675–9688. https://doi.org/10.1021/acsomega.8b01330 (2018).
6. Teju, M. D. & Majamo, S. L. Synthesis and application of lanthanum-doped magnetic biochar composite adsorbent for removal of fluoride from water. *Environ. Monit. Assess.* **195**, 1469. https://doi.org/10.1007/s10661-023-12075-y (2023).
7. Ebsa, D. G. Defluoridation of drinking water by modified natural zeolite with Cationic surfactant, in the case of Ziway town, Ethiopia. *Clean Eng, Technol,* **12**, 100596. https://doi.org/10.1016/j.clet.2023.100596 (2023).
8. Fito, J., Said, H., Feleke, S. & Worku, A. Fluoride removal from aqueous solution onto activated carbon of Catha edulis through the adsorption treatment technology. *Environ. Syst. Res.* **8**, 1–10. https://doi.org/10.1186/s40068-019-0153-1 (2019).
9. Kamble, S. P., Dixit, P., Rayalu, S. S. & Labhsetwar, N. K. Defluoridation of drinking water using chemically modified bentonite clay. *Desalination* **249**, 687–693. https://doi.org/10.1016/j.desal.2009.01.031 (2009).
10. Gao, Y., Li, M., Ru, Y. & Fu, J. Fluoride removal from water by using micron zirconia/zeolite molecular sieve: Characterization and mechanism. *Groundw. Sustain. Dev.* **13**, 100567. https://doi.org/10.1016/j.gsd.2021.100567 (2021).
11. Afzal, M. Z. et al. Removal of ciprofloxacin via enhancing hydrophilicity of membranes using biochar. *Appl. Water Sci.* **14**, 195. https://doi.org/10.1007/s13201-024-02270-8 (2024).
12. Sairam Sundaram, C., Viswanathan, N. & Meenakshi, S. Defluoridation of water using magnesia/chitosan composite. *J. Hazard Mater.* **163**, 618–624. https://doi.org/10.1016/j.jhazmat.2008.07.009 (2009).
13. Tabi, R. N. et al. Zeolite synthesis and its application in water defluorination. *Mater. Chem. Phys.* **261**, 124229. https://doi.org/10.1016/j.matchemphys.2021.124229 (2021).
14. Haldar, D., Duarah, P. & Purkait, M. K. MOFs for the treatment of arsenic, fluoride and iron contaminated drinking water: A review. *Chemosphere* **251**, 126388. https://doi.org/10.1016/j.chemosphere.2020.126388 (2020).
15. Tan, T. L., Krusnamurthy, P. A., Nakajima, H. & Rashid, S. A. Adsorptive, kinetics and regeneration studies of fluoride removal from water using zirconium-based metal organic frameworks. *RSC Adv.* **10**, 18740–18752. https://doi.org/10.1039/d0ra01268h (2020).
16. Khatamian, M., Afshar No, N., Hosseini Nami, S. & Fazli-Shokouhi, S. Synthesis and characterization of zeolite A, Fe_3O_4/zeolite A, and Fe_2O_3/zeolite A nanocomposites and investigation of their arsenic removal performance. *J. Iran. Chem. Soc.* **20**, 1657–1670. https://doi.org/10.1007/s13738-023-02787-w (2023).
17. Derbe, T., Zereffa, E. A. & Sani, T. Synthesis of zeolite-A/Fe_3O_4/biochar composite for removal of Cr(VI) from aqueous solution. *Int. J. Environ. Sci. Technol.* https://doi.org/10.1007/s13762-024-05642-4 (2024).
18. Sani, T., Gómez-Hortigüela, L., Pérez-Pariente, J., Chebude, Y. & Díaz, I. Defluoridation performance of nano-hydroxyapatite/stilbite composite compared with bone char. *Sep. Purif. Technol.* **157**, 241–248. https://doi.org/10.1016/j.seppur.2015.11.014 (2016).
19. Derbe, T., Gindose, T. G., Sani, T. & Zereffa, E. A. Synthesis of zeolite-A/Fe_3O_4/biochar/MOF-5 composite for the defluoridation of drinking water. *Appl. Water Sci.* **15**, 161. https://doi.org/10.1007/s13201-025-02438-w (2025).
20. Zhou, N. et al. Enhanced fluoride removal from drinking water in wide pH range using La/Fe/Al oxides loaded rice straw biochar. *Water Supply* **22**, 779–794. https://doi.org/10.2166/ws.2021.232 (2022).
21. Zheng, X. J. et al. Assessment of zeolite, biochar, and their combination for stabilization of multimetal-contaminated soil. *ACS Omega* **5**, 27374–27382. https://doi.org/10.1021/acsomega.0c03710 (2020).
22. Zhang, J. et al. Adsorption properties of magnetic magnetite nanoparticle for coexistent Cr(VI) and Cu(II) in mixed solution. *Water* **12**, 446. https://doi.org/10.3390/w12020446 (2020).
23. Shemy, M. H. et al. Synthesis of green magnetite/carbonized coffee composite from natural pyrite for effective decontamination of congo red dye: Steric, synergetic, oxidation, and ecotoxicity studies. *Catalysts* **13**, 264. https://doi.org/10.3390/catal13020264 (2023).
24. Tran, N. B. T., Duong, N. B. & Le, N. L. Synthesis and characterization of magnetic Fe_3O_4/Zeolite NaA nanocomposite for the adsorption removal of methylene blue potential in wastewater treatment. *J. Chem.* **2021**, 6678588. https://doi.org/10.1155/2021/6678588 (2021).
25. Saeed, A. A. H. et al. Pristine and magnetic kenaf fiber biochar for Cd^{2+} adsorption from aqueous solution. *Int. J. Environ. Res. Public Health* **18**, 7949. https://doi.org/10.3390/ijerph18157949 (2021).
26. Vo, A. T. et al. Efficient removal of Cr(VI) from water by biochar and activated carbon prepared through hydrothermal carbonization and pyrolysis: Adsorption-coupled reduction mechanism. *Water* **11**, 1164. https://doi.org/10.3390/w11061164 (2019).
27. Assirey, E. A. & Altamimi, L. R. Chemical analysis of corn cob-based biochar and its role as water decontaminants. *J. Taibah Univ. Sci.* **15**, 111–121. https://doi.org/10.1080/16583655.2021.1876350 (2021).
28. Ghaffar, A., Zhu, X. & Chen, B. Biochar composite membrane for high performance pollutant management: Fabrication, structural characteristics and synergistic mechanisms. *Environ. Pollut.* **233**, 1013–1023. https://doi.org/10.1016/j.envpol.2017.09.099 (2018).
29. Fito, J., Abewaa, M. & Nkambule, T. Magnetite-impregnated biochar of parthenium hysterophorus for adsorption of Cr(VI) from tannery industrial wastewater. *Appl. Water Sci.* **13**, 78. https://doi.org/10.1007/s13201-023-01880-y (2023).
30. Pan, X., Gu, Z., Chen, W. & Li, Q. Preparation of biochar and biochar composites and their application in a Fenton-like process for wastewater decontamination: A review. *Sci. Total Environ.* **754**, 142104. https://doi.org/10.1016/j.scitotenv.2020.142104 (2021).
31. Mosa, A., El-Ghamry, A. & Tolba, M. Biochar-supported natural zeolite composite for recovery and reuse of aqueous phosphate and humate: Batch sorption–desorption and bioassay investigations. *Environ. Technol. Innov.* **19**, 100807. https://doi.org/10.1016/j.eti.2020.100807 (2020).
32. Kong, F. et al. Removal of Cr(VI) from wastewater by artificial zeolite spheres loaded with nano Fe–Al bimetallic oxide in constructed wetland. *Chemosphere* **257**, 127224. https://doi.org/10.1016/j.chemosphere.2020.127224 (2020).
33. Kosmulski, M. The pH dependent surface charging and points of zero charge. IX. Update. *Adv. Colloid Interface Sci.* **296**, 102519. https://doi.org/10.1016/j.cis.2021.102519 (2021).
34. Tolkou, A. K. & Zouboulis, A. I. Fluoride removal from water sources by adsorption on MOFs. *Separations* **10**, 467. https://doi.org/10.3390/separations10090467 (2023).
35. Hussein, I. A. & Vegi, M. R. Defluoridation of drinking water using coalesced and un-coalesced mica. *Appl. Water Sci.* **10**, 64. https://doi.org/10.1007/s13201-020-1153-z (2020).
36. Jung, K. W., Choi, B. H., Jeong, T. U. & Ahn, K. H. Facile synthesis of magnetic biochar/Fe_3O_4 nanocomposites using electromagnetization technique and its application on the removal of acid orange 7 from aqueous media. *Bioresour. Technol.* **220**, 672–676. https://doi.org/10.1016/j.biortech.2016.09.035 (2016).

37. Ahmad, M. et al. Date palm waste-derived biochar composites with silica and zeolite: Synthesis, characterization and implication for carbon stability and recalcitrant potential. *Environ. Geochem. Health* **41**, 1687–1704. https://doi.org/10.1007/s10653-017-9947-0 (2019).
38. Kumari, S., Singh, N., Sharma, R., Yadav, M. & Khan, S. Kinetics and isotherms of adsorption of fluoride onto Fe_3O_4/graphene/alginate nanocomposite hydrogel. *Environ. Nanotechnol. Monit. Manag.* **16**, 100590. https://doi.org/10.1016/j.enmm.2021.100590 (2021).
39. Santhosh, C. et al. Synthesis and characterization of magnetic biochar adsorbents for the removal of Cr(VI) and Acid orange 7 dye from aqueous solution. *Environ. Sci. Pollut. Res.* **27**, 32874–32887. https://doi.org/10.1007/s11356-020-09275-1 (2020).
40. Cao, J., Sun, Q., Wang, P., Shen, J. & Dai, X. Synthesize and characterize of Fe_3O_4/zeolite 4A magnetic nanocomposite. *J. Dispers. Sci. Technol.* **43**, 517–525. https://doi.org/10.1080/01932691.2020.1843480 (2022).
41. Ayele Regassa, L. Synthesis and characterization of zeolite A from Kaolin of Ethiopia: Studies of its application as detergent builder and in tannery wastewater treatment (2016).
42. Belachew, N. & Hinsene, H. Preparation of zeolite 4A for adsorptive removal of methylene blue: Optimization, kinetics, isotherm, and mechanism study. *SILICON* **14**, 1629–1641. https://doi.org/10.1007/s12633-020-00938-9 (2022).
43. Kokab, T. et al. Effective removal of Cr(Vi) from wastewater using biochar derived from walnut shell. *Int. J. Environ. Res. Public Health* **18**, 9670. https://doi.org/10.3390/ijerph18189670 (2021).
44. Massoudinejad, M., Ghaderpoori, M., Shahsavani, A. & Amini, M. M. Adsorption of fluoride over a metal organic framework Uio-66 functionalized with amine groups and optimization with response surface methodology. *J. Mol. Liq.* **221**, 279–286. https://doi.org/10.1016/j.molliq.2016.05.087 (2016).
45. Behailu, T. W., Badessa, T. S. & Tewodros, B. A. Analysis of physical and chemical parameters in ground water consumed within Konso area, Southwestern Ethiopia. *Afr. J. Environ. Sci. Tech.* **12**, 106–114. https://doi.org/10.5897/ajest2017.2419 (2018).

Acknowledgements
The authors would like to thank Wachemo University and Addis Ababa Science & Technology University for their providing materials.

Author contributions
T.D.: Writing original draft, Methodology, Data curation, Conceptualization. Y.T.: Formal analysis, Data curation. T.S.: Resources, methodology, Conceptualization. E.A.Z.: Writing & editing, Supervision, Investigation, Conceptualization.

Funding
This work is partly supported by the Addis Ababa Science and Technology University project grant code IG 08/2021.

Declarations

Competing interests
The authors declare no competing interests.

Additional information
Supplementary Information The online version contains supplementary material available at https://doi.org/10.1038/s41598-025-31370-x.

Correspondence and requests for materials should be addressed to T.S.

Reprints and permissions information is available at www.nature.com/reprints.

Publisher's note Springer Nature remains neutral with regard to jurisdictional claims in published maps and institutional affiliations.